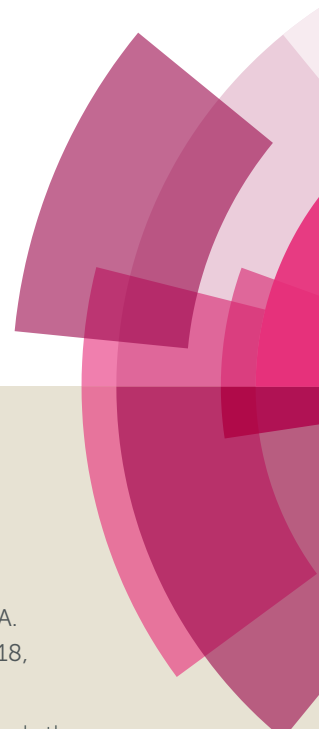


NJC

Accepted Manuscript



This article can be cited before page numbers have been issued, to do this please use: S. Gaonkar, M. A. Savanur, M. G. Sunagar, B. Puthusseri, N. Deshapande, A. A. Nadaf and I. A. M. Khazi, *New J. Chem.*, 2018, DOI: 10.1039/C7NJ04157H.



This is an Accepted Manuscript, which has been through the Royal Society of Chemistry peer review process and has been accepted for publication.

Accepted Manuscripts are published online shortly after acceptance, before technical editing, formatting and proof reading. Using this free service, authors can make their results available to the community, in citable form, before we publish the edited article. We will replace this Accepted Manuscript with the edited and formatted Advance Article as soon as it is available.

You can find more information about Accepted Manuscripts in the [author guidelines](#).

Please note that technical editing may introduce minor changes to the text and/or graphics, which may alter content. The journal's standard [Terms & Conditions](#) and the ethical guidelines, outlined in our [author and reviewer resource centre](#), still apply. In no event shall the Royal Society of Chemistry be held responsible for any errors or omissions in this Accepted Manuscript or any consequences arising from the use of any information it contains.

Exploring the potential of newly synthesized 4-methyl-6-morpholinopyrimidine derivatives as antiproliferative agents

Supreet Gaonkar^{a,1}, Mohammed Azharuddin Savanur^{b,c,1}, Manjunath G. Sunagar^a, Bijesh Puthusseri^d, Narahari Deshapande^a, Afra A. Nadaf^a, Imtiyaz Ahmed M. Khazi^{a,*}

^a Department of Studies in Chemistry, Karnatak University, Dharwad 580003, Karnataka, India.

^b Department of Biochemistry, Karnatak University, Dharwad 580003, Karnataka, India.

^c Present Address: Indian Institute of Science, Bangalore 560012, India.

^d CSIR-Central, Food Technological Research Institute, Mysore 570020, India.

¹ These authors contributed equally to this work

*Corresponding author, Imtiyaz Ahmed M. Khazi; Email: drimkorgchem@gmail.com

Abstract

In view of exploring the potential of pyrimidine derivatives as anticancer agents, a series of 4-methyl-6-morpholinopyrimidine derivatives were synthesised and characterised by NMR (¹H & ¹³C), SC-XRD and Mass spectral analysis. The *in vitro* anticancer activity of these compounds was investigated using different human cancer cell lines namely HeLa (cervix), NCI-H460 (lung), MCF-7(breast), HepG2 (liver) and IMR-32 (brain). Compounds 4c and 5h exhibited potent anticancer activity in dose dependent manner as compared to other derivatives, with an IC₅₀ values of 5.88 ± 1.22 and 6.11 ± 2.12 μM on HeLa and NCI-H460 cells respectively. The inhibitory effect of 4c and 5h on cancer cell proliferation was shown to be a consequence of reactive oxygen species (ROS) generation and subsequent induction of cellular apoptosis, as evidenced by increase in hypodiploid (subG1) population, early apoptotic cell population, caspase-3/7 activity, loss of mitochondrial membrane potential and degradation of nuclear DNA. Furthermore, molecular docking studies revealed that 4c and 5h compounds binds to ATP binding pocket of mammalian target of rapamycin (mTOR). Based on our results we objectify that 4-methyl-6-morpholinopyrimidine derivatives prevent cancer cell proliferation by inducing apoptosis and thus have potential to be further explored for anticancer properties.

Keywords: Morpholinopyrimidine; Anti-proliferative; Cytotoxic; Apoptosis; mTOR

1. Introduction

Cancer is a multifactorial disease with high rate of mortality. Lung, liver, prostate, stomach and colorectal cancer are the most common types of cancer in men, while breast, cervix, colorectal, lung and stomach cancer are common among women.¹ Development of cancer in humans is a multistep process that includes generating persistent growth signals and insensitivity to anti-growth signals, evasion of apoptosis, unlimited replication potential, angiogenesis, invasion and metastasis.² The discovery of targeted-drug therapies that intervene the cancer development process has patently impeded malignancies.³ However, the alarming rise of new types of cancer and advanced metastasized cancer remains untreatable. Hence, a continued search for development of selective, more potent and less toxic chemotherapeutic agents is needed for the treatment of cancer.

Organic moieties specifically those containing a hetero atom in their aromatic nucleus have added to the growth in the library of bioactive compounds and have shown wide applications in medicinal chemistry fields. According to the FDA (Food and Drug Administration) database, nitrogen containing heterocyclic compounds are seen in approximately 60% of the small molecule drugs which proves the significance of nitrogen based heterocycles.⁴ Pyrimidines are the most important six membered aromatic heterocyclic compounds widely distributed in nature as nucleotides, thiamine and alloxan, whereas barbiturates are one of their earliest synthetic forms. There are numerous reports available in literature, which has shown that pyrimidine libraries against some biological targets have contributed significantly to the development of pharmacologically active agents.⁵⁻⁷ Synthetic pyrimidine derivatives exhibits remarkable pharmacological activities and form a component in a number of useful drugs, which are associated with many biological and therapeutic activities.⁸ In particular, pyrimidine derivatives are found to act as anticancer,⁹ anti-HIV,¹⁰ antibacterial,¹¹ antihypertensive,¹² anticonvulsant,¹³ antitubercular,¹⁴ analgesic¹⁵ and antiplasmodial agents.¹⁶ Among the literature reports of pyrimidines, anticancer activity is more extensively studied. Because of the vast diversity in its chemistry, researchers are working in the synthesis of substituted pyrimidines as anticancer agents. Some of the pyrimidine based anticancer drugs approved by FDA are 5-Flurouracil, Tegafur, Osimeritinib, Idelalisib, Afatinib, Palbocilib, Ceritinib etc.,

Morpholine is the most commonly used heterocyclic secondary amine substituent in drugs and pharmaceutically active compounds.¹⁷ Morpholine and pyrimidine hybrids gained

attention of medicinal chemist because of their therapeutic application as antitumor,¹⁸ antimicrobial,¹⁹ anti-inflammatory,²⁰ antisenility²¹ and antimalarial agents.²² Morpholinopyrimidines are biologically important molecules, mainly studied as PI3K/Akt/mTOR pathway inhibitors.²³⁻²⁵ Many of these PI3K/mTOR inhibitors share morpholinopyrimidine as common structural unit such as Apatolisib (GDC-0980),²⁶ Pictilisib (GDC-0941),²⁷ PI-103,²⁸ GNE-477²⁹ and so on (Fig. 1).

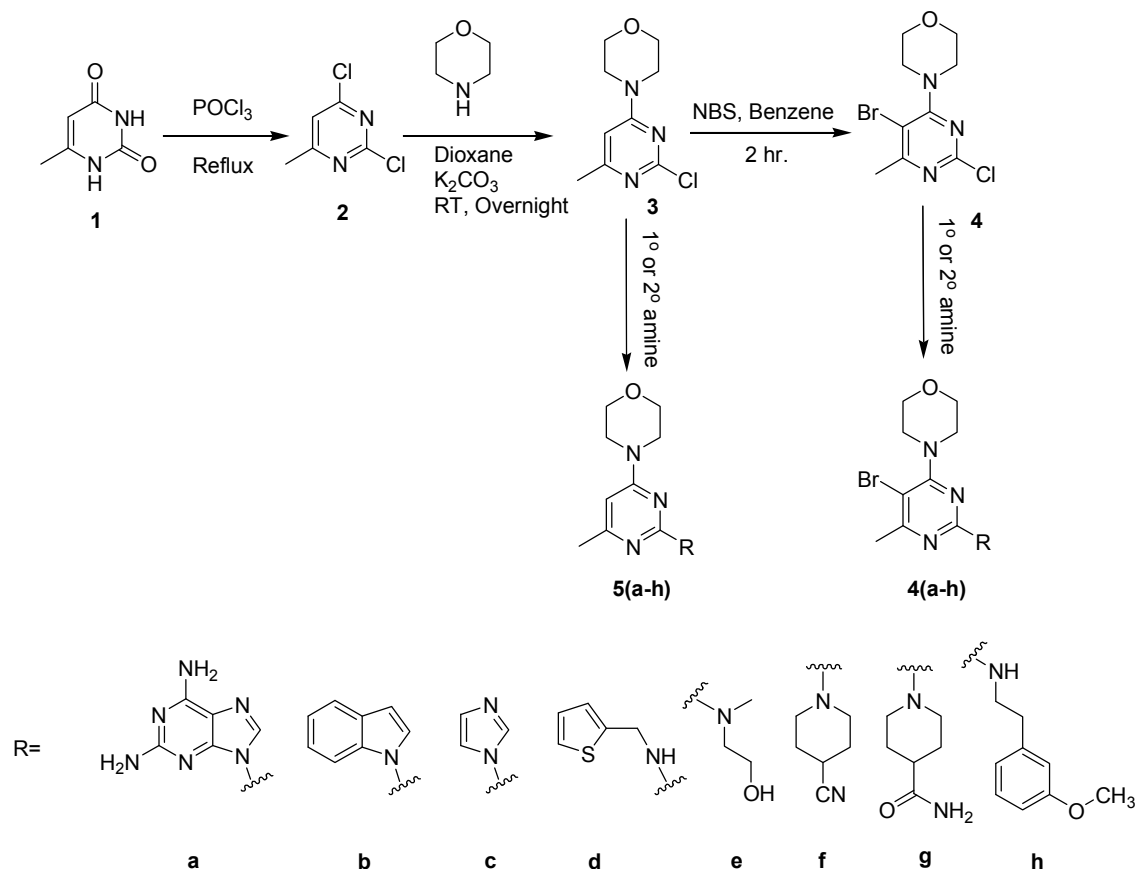
In the present study we report synthesis and cytotoxicity of 4-methyl-6-morpholinopyrimidine derivatives against different cancer cell lines. In addition, this report also explains the mechanism of morpholinopyrimidine derivatives induced cell death by generation of ROS and subsequent induction of cellular apoptosis, as well as their interaction with mTOR as possible target.

2. Result and Discussion

2.1 Chemistry

The synthetic routes for 4-methyl-6-morpholinopyrimidine derivatives (**4a-4h** & **5a-5h**) are outlined in **Scheme 1**. 2,4-dichloro-6-methylpyrimidine (**2**) was synthesised by treating 6-methylpyrimidine-2,4(1H,3H)-dione (**1**) and phosphorusoxychloride under reflux temperature followed by the neutralisation with sodium bicarbonate. The key intermediate 2-chloro-4-methyl-6-morpholinopyrimidine (**3**) was synthesised by reacting **2** with morpholine and potassium carbonate in dioxane at room temperature. Bromination of **3** was done by N-bromosuccinimide in benzene to afford 5-bromo-2-chloro-4-methyl-6-morpholinopyrimidine (**4**). The target compounds **4(a-h)** and **5(a-h)** are synthesised with good yield by nucleophilic substitution reaction of various amines (**a-h**) with either **4** or **3** respectively. Structures of the synthesized compounds were characterised by ¹H NMR, ¹³C NMR and Mass spectral analysis. Structure of compound **4a** was supported by NMR spectral studies, the characteristic singlet at 8.89 ppm and a broad singlet at 5.71 ppm for two protons due to C8-H of purine and C2-NH₂ of purine respectively. Further the formation of compound **4a** was confirmed by LC-MS data. The ¹H NMR spectrum of compound **4c** shows three characteristic singlets at 8.53 ppm 7.77 ppm and 7.10 ppm due to C2-H, C5-H and C4-H of imidazole respectively. Two triplets at 3.83 ppm for four protons and 3.67 ppm for four protons corresponding to two CH₂ groups next to oxygen atom and two CH₂ group next to nitrogen atom of morpholine respectively, it is further supported by ¹³C NMR and Mass spectral data. Structure of the compound **4h** was confirmed by single crystal X-ray analysis.

A characteristic singlet at 6.20 ppm due to C5-H of pyrimidine supports the formation of compound **5c** and it is confirmed by ^{13}C NMR and Mass spectral data.



Scheme 1: Synthesis of 4-methyl-6-morpholinopyrimidine derivatives

2.2. Single crystal X-ray analysis

A suitable single crystal was collected through the polarising microscope and mounted on the 'Bruker APEX-II CCD' diffractometer system is equipped with micro focus sealed tube Mo source, CCD area detector. Crystal was kept at 298K (2) during the data collection with scan width of 0.5mm and distance of 45mm from crystal to detector. The structure (Fig. 2) was solved using the Olex2 with the XT,³⁰ using Intrinsic Phasing and refined with the ShelXL refinement package using Least Squares minimization.³¹ The molecule crystallizes in the monoclinic crystal system having a centrosymmetric space group i.e. $P2_1/n$ and one molecule in the asymmetric unit. In the crystal structure Br...Br (3.590 Å) Br... π (3.491 Å) and also CH... π (2.892 Å) interaction makes the molecule more stable (Fig. 3). Crystal data are listed in the **Table 1**.

Table 1: Crystal data and structure refinement of compound **4h**.

Empirical formula	C ₁₈ H ₂₃ BrN ₄ O ₂
Formula weight	407.31
Temperature/K	293(2)
Crystal system	Monoclinic
Space group	P2 ₁ /n
a/Å	18.8570(6)
b/Å	4.98220(10)
c/Å	21.8645(7)
α/°	90
β/°	115.2770(10)
γ/°	90
Volume/Å ³	1857.48(9)
Z	4
ρ _{calc} /cm ³	1.457
μ/mm ⁻¹	2.232
F(000)	840.0
Crystal size/mm ³	0.26 × 0.25 × 0.24
Radiation	MoKα (λ = 0.71073)
2θ range for data collection/°	8.264 to 49.998
Index ranges	-22 ≤ h ≤ 22, -5 ≤ k ≤ 5, -25 ≤ l ≤ 25
Reflections collected	48066
Independent reflections	3212 [R _{int} = 0.0341, R _{sigma} = 0.0137]
Data/restraints/parameters	3212/0/228
Goodness-of-fit on F ²	1.131
Final R indexes [I ≥ 2σ (I)]	R ₁ = 0.0393, wR ₂ = 0.1106
Final R indexes [all data]	R ₁ = 0.0437, wR ₂ = 0.1144
Largest diff. peak/hole / e Å ⁻³	0.48/-0.90
CCDC number	1478498

2.3. *In vitro* Anticancer activity

2.3.1. Morpholinopyrimidine compounds inhibit proliferation of cancer cells

Cytotoxicity of newly synthesized 4-methyl-6-morpholinopyrimidine derivatives was determined *in-vitro* on HeLa, NCI-H460, MCF-7, HepG2 and IMR-32 cell lines by using MTT assay. The IC₅₀ (μM) values (concentration required to inhibit 50% of cancer cell proliferation) of the tested compounds and the standard reference doxorubicin are listed in **Table 2**. The results of cell viability assay showed strong growth inhibitory effect of Morpholinopyrimidine compounds on cancer cells in dose dependent manner. Compounds **4c** and **5h** showed higher activity as compared to other derivatives, with an IC₅₀ values of 5.88 ± 1.22 and 6.11 ± 2.12 μM on HeLa and NCI-H460 cells respectively. The dose dependent cytotoxic effect of **4c** and **5h** was observed in HeLa and NCI-H460 cells, where at 20 μM

compound **4c** (Fig. 4A) caused $86.2 \pm 3.44\%$ ($P < 0.0001$) and $79.3 \pm 4.2\%$ ($P < 0.0001$), and compound **5h** (Fig. 4B) caused $75.2 \pm 3.8\%$ ($P < 0.0001$) and $84.3 \pm 3.34\%$ ($P < 0.0001$) growth inhibition in HeLa and NCI-H460 cells respectively, suggesting the cytotoxic effect of Morpholinopyrimidine compounds (**4c** and **5h**) is dose dependent. Considering the potent cytotoxic effect of **4c** and **5h** on HeLa and NCI-H460 cells, respectively, the effect of compound **4c** and **5h** on morphology of cancer cells was determined. Cancer cells in control group had distinct, well defined morphology with clear skeletons; In contrast cells treated with **4c** and **5h** compounds had indecisive morphology with indistinct skeletons and appeared to be dead as evidenced by phase contrast images (Fig. 4C), demonstrating the cytotoxic effect of these compounds.

From table 2 it is evident that compounds comprising imidazole (**4c**) and 2-(3-methoxyphenyl) ethanamine (**5h**) at C-2 position of the pyrimidine are more potent as compared to remaining derivatives. The antiproliferative activity of compound **4c** and **5c** in HeLa cell line is attributed due to the presence of imidazole ring. Since imidazole ring has structural resembles with histidine, it can easily binds with proteins compared to other heterocyclic rings. Many of the anticancer compounds are having imidazole skeleton as structural backbone.^{32,33} Compound **5h** and **4h** have shown good and moderate activity against NCIH-460 cell lines respectively. The compounds having ethanamine and ethylenediamine linkage with conformational flexibility have been important pharmacophore in many biologically significant molecules. This could be the possible reason for the enhanced activity.³⁴ Compounds **4a**, **4b**, **5a** & **5b** showed low solubility and are less potent than the remaining derivatives of morpholinopyrimidine (**4d**, **4e**, **4f**, **4g**, **4h**, **5c**, **5d**, **5e**, **5f**, **5g**) which are moderately active.

Table 2 : Anti-proliferative activity of Morpholino pyrimidine compounds on HeLa, NCI-H460, MCF-7, HepG2 and IMR-32 cell lines was determined by MTT assay and the IC₅₀ values were calculated based on results obtained at 24-h time point.

IC ₅₀ values (μM) of Morpholino pyrimidine derivatives					
Compounds	HeLa	NCI-H460	MCF-7	HepG2	IMR-32
4a	>20	>20	>20	>20	>20
4b	>20	16.92 ± 3.30	>20	19.88 ± 3.41	>20
4c	5.88 ± 1.22	11.34 ± 2.63	12.99 ± 2.30	14.12 ± 3.78	13.63 ± 2.94

4d	13.69 ± 1.93	>20	16.46 ± 1.02	15.84 ± 2.36	16.05 ± 1.40
4e	12.61 ± 3.78	16.84 ± 3.63	15.69 ± 0.89	14.35 ± 1.91	>20
4f	12.72 ± 2.12	15.27 ± 2.69	14.93 ± 4.32	>20	16.72 ± 3.68
4g	>20	>20	>20	>20	>20
4h	16.04 ± 0.93	12.98 ± 2.68	17.34 ± 2.38	16.44 ± 3.07	17.28 ± 4.12
5a	>20	>20	19.81 ± 2.08	>20	18.03 ± 2.36
5b	>20	>20	>20	>20	>20
5c	12.09 ± 1.68	14.77 ± 2.89	13.52 ± 2.10	12.84 ± 3.27	15.74 ± 0.93
5d	17.46 ± 3.02	16.37 ± 2.16	15.92 ± 1.68	14.56 ± 1.74	15.53 ± 1.73
5e	16.69 ± 2.92	10.28 ± 3.01	17.17 ± 4.13	13.91 ± 2.97	>20
5f	17.63 ± 4.37	16.19 ± 1.05	16.60 ± 1.36	>20	14.49 ± 1.89
5g	15.96 ± 2.03	14.06 ± 2.32	16.11 ± 2.60	18.41 ± 1.09	>20
5h	10.02 ± 1.39	6.11 ± 2.12	11.69 ± 3.62	13.32 ± 2.34	14.56 ± 1.92

2.3.2. Compounds **4c** and **5h** induce accumulation of HeLa cells in hypodiploid (subG1) phase of cell cycle.

The effects of cytotoxic compounds are mainly exerted by arresting the cells at specific phase of a cell cycle, thus preventing cellular proliferation and inducing cell death.³⁵⁻³⁷ The population of cells undergoing apoptosis are represented as the hypodiploid population in the subG1 phase.^{38,39} Distribution of cells in the different phases of cell cycle was determined by exposing HeLa and NCI-H460 cells to **4c** and **5h** compounds respectively at different concentrations, followed by propidium iodide (PI) staining and flow cytometry analysis. Cells treated with compounds **4c** and **5h** showed a dose dependent increase in hypodiploid population, where treatment with 10 μ M of compounds resulted in 27.3% and 28.6% respectively, which increased to 39.7% and 40.9%, respectively at 20 μ M as compared to 1.5% and 1.8% respectively in control groups, suggesting that these molecules promote cell death through induction of apoptosis (Fig. 5A). The percentage of cell populations in each phase of cell cycle is represented in the bar diagram (Fig. 5B and 5C).

2.3.3. Induction of apoptosis by compound **4c** and **5h**.

Phosphatidylserine translocation to the outer surface of plasma membrane is a hallmark of apoptosis,^{40,41} which can be detected using Annexin-V.^{42,43} The potential of compound **4c** and **5h** to induce apoptosis was determined by Annexin-V and PI staining, distinguishes viable, early and late apoptosis or dead cells. HeLa and NCI-H460 cells

exposed to **4c** and **5h** compounds at different concentration showed dose dependent increase in early and late apoptotic population. As shown in Fig. 6A, a significant increase in early apoptotic cells (Annexin-V positive) 52.7% and 50.2% was observed after treatment with **4c** and **5h** compounds respectively, as compared to 0.5% and 1.1% in control groups, respectively. There was also a dose dependent increase in late apoptotic cells (Annexin-V and PI positive) 32.2% and 33.8% respectively, indicating that these compounds induces cellular apoptosis in a dose dependent manner. Percentage of cells in four different quadrants as shown in Fig. 6B and 6C was represented as bar graph.

2.3.4. Intracellular ROS production by compound **4c** and **5h**.

Excessive amount of ROS can cause oxidative damage to biomolecules, inducing apoptosis and cell death.^{44,45} Thus, compounds that exhibit a potent ROS generating ability in cancer cells show promising anticancer activity.⁴⁶⁻⁴⁸ The ability of compound **4c** and **5h** to generate ROS in cancer cells was determined by staining with DCFDA-H2, a non-fluorescent dye which upon oxidation by ROS emits green fluorescence. Results of fluorescence microscopy revealed that cells treated with **4c** and **5h** showed increase in green fluorescence as compared to control cells, indicating that these compounds promote ROS generation and induce apoptosis in cancer cells (Fig. 8A).

2.3.5. Compound **4c** and **5h** induce loss of mitochondrial membrane potential.

Increase in intracellular ROS causes mitochondrial damage and loss in mitochondrial membrane potential, further leading to apoptosis.^{49,50} Since, compound **4c** and **5h** induced intracellular ROS production, the detrimental effects of elevated ROS levels on mitochondria were analysed by measuring the changes in mitochondrial membrane potential. The effect of **4c** and **5h** on the mitochondrial membrane potential was determined by staining cells with Jc-1 dye, which accumulates in intact mitochondria emitting red fluorescence. The accumulation of JC-1 is membrane potential dependent and can be explored to measure changes in mitochondrial polarisation. During apoptosis, mitochondrial depolarisation leads to collapse of mitochondrial membrane potential, where JC-1 accumulates in cytoplasm emitting green fluorescence.⁵¹ An increase in the number of cells which are positive for green fluorescence after treatment with **4c** and **5h** compounds at various concentrations (0-20 μ M) was observed (Fig. 7A), suggesting that the Compound **4c** and **5h** induced cell death involves mitochondrial depolarisation associated apoptosis. The percentage of cell populations with

high and low mitochondrial membrane potential are represented in the bar diagram (Fig. 7B and 7C).

2.3.6. Activation of effector caspase-3/7 by Compound **4c** and **5h**.

The ultimate consequence of elevated ROS is oxidative stress mediated induction of apoptosis.^{52,53} As the activation of effector caspase-3/7 brings about the characteristic changes associated with apoptosis like DNA condensation and fragmentation, the potential of compound **4c** and **5h** to activate effector caspases was determined using appropriate substrates provided in caspase-activity detection kit. As shown in Fig. 8B, a significant increase in caspase 3/7 activity (1.96 and 3.25 fold) was observed in cells treated with **4c** and **5h** compounds respectively when compared to untreated control, indicating that cell death caused by these compounds is linked to induction of cell apoptosis.

2.4. Compound **4c** and **5h** causes chromatin condensation and DNA fragmentation

Nuclear shrinkage, chromatin condensation and fragmented DNA, are the remarkable features of cellular apoptosis. Anti-cancer drugs are known to induce DNA fragmentation by activation of specific endonucleases which leads to cancer cell death.^{54,55} As compound **4c** and **5h** induced apoptotic cell death in cancer cells, we further investigated the ability of these compounds to condense chromatin and fragment DNA, in order to determine their mechanism to induce cell death. As shown in Fig. 8D, DAPI-staining confirmed significant chromatin condensation in Morpholino pyrimidine compounds treated cells, suggesting induction of apoptosis. DNA strand breaks in cells exposed to **4c** and **5h** compounds was analysed by agarose gel electrophoresis, where the treatment of **4c** and **5h** resulted in a fragmented DNA ladder formation in a dose-dependent manner (Fig. 8C), further supporting the evidence that these compounds induced cell death via induction of apoptosis.

2.5 Compound **4c** and **5h** binds to the ATP pocket of the mTOR

The ligands, **4c** and **5h**, docked into the catalytic domain of the mTOR, and the best docked conformation is provided in (Fig. 9). Molecule **4c** was found to have ligand-interactions with the amino acids Asn247, Ala311, Ile298 and Glu296 of the modelled mTOR. The hydrophobic morpholino moiety of the **4c** ligand was found to fit in the hydrophobic pocket of the mTOR binding sites constituted by Ile298, Pro309, Leu306, Phe301, Ala 311, Leu312 and Leu 250. Whereas, the hydrophilic pyrimidine end of the **4c** molecule was aligned towards the hydrophilic pocket constituted by the amino acids Lys256,

Asn254, Met251, Glu310, Arg249 and Trp248 of the pharmacophore. Molecule **5h** has shown interactions with Glu9, Asp10, Gln13, Asp14, Asp176 and Asp252. The ligand, **5h**, was found to have its hydrophobic morpholine end docked in the hydrophobic pocket of the binding site mainly constituted by the Val183, Gly178, Phe240, Leu246 and Gly291 of the pharmacophore model. Whereas, the hydrophilic pyrimidine moieties of the **5h** ligand was aligned towards the hydrophilic pocket constituted by the amino acids Glu13, Glu9, His8, Asp10, Arg12, Thr292, Trp248 and Asp176 of the mTOR catalytic domain. Previous studies for screening mTOR inhibitors have noted the binding of ligands in the same binding site with similar attributes.⁵⁶⁻⁵⁸ They have pointed out the importance of hydrogen bond acceptor ability of bridged morpholine for the high activity of these inhibitors. Our study shows the structural features for the activity of morpholinopyrimidine as mTOR kinase inhibitors. The study also shows the possible sites of modifications for improving the activity of these inhibitors.

3. Conclusion

In summary, a series of sixteen 4-methyl-6-morpholinopyrimidine derivatives were synthesized and their cytotoxic potential was evaluated using different human cancer cells. Within the series, compound **4c** and **5h** exhibited strong growth inhibitory effect in a dose dependent manner with IC₅₀ values of 5.88 ± 1.22 and 6.11 ± 2.12 μM on HeLa and NCI-H460 cells respectively. The structure and activity relationship analysis revealed that compounds consisting imidazole and 2-(3-methoxyphenyl) ethanamine at C-2 position of the pyrimidine are more potent and showed pronounced cytotoxicity. Therefore, compound **4c** and **5h** were selected for further studies to determine the mechanism of action. The cell cycle analysis, annexin-V/PI assay, assessment of caspase-3/7 activity, evaluation of mitochondrial membrane potential and DNA damage studies were carried out to determine the mechanistic details of morpholinopyrimidine derivatives induced cancer cell death. The results of these studies indicate that the observed anti-proliferative activity of **4c** and **5h** compounds on cancer cells is a consequence of cellular apoptosis induction. Furthermore, molecular docking of **4c** and **5h** compounds with mTOR shows that **4c** and **5h** compounds bind to ATP binding pocket of the kinase. Based on the results obtained we conclude that 4-methyl-6-morpholinopyrimidine derivatives can be further explored for anticancer properties and will be studied as plausible mTOR inhibitors.

4. Experimental

4.1 Chemistry

4.1.1. Materials and Method

All the solvents and reagents are of analytical grade and were used directly without further purification. Thin layer chromatography (TLC) technique was employed to monitor the progress of reaction. Merck Silica gel 60 F₂₅₄ TLC plates were used and spots were visualized using ultraviolet light (254 nm) or iodine chamber. Column chromatography was carried out with silica gel 60 (100-200 mesh). Melting points were determined by open capillary method and are uncorrected. ¹H NMR and ¹³C NMR spectra were recorded on Bruker 400 MHz and 101 MHz FT NMR spectrometer respectively, in DMSO-D₆ and CDCl₃ by using tetramethylsilane (TMS) as internal standard. Chemical shifts are expressed in ppm (δ) and multiplicities of NMR signals are assigned as s (singlet), d (doublet), t (triplet), q (quartet), bs (broad singlet), dt (doublet of triplet), tt (triplet of triplet), dq (doublet of quartet), m (multiplet, for unresolved lines), etc. Mass spectra were recorded using Shimadzu GCMS-QP2010S

4.1.2. General procedure for synthesis of (4a & 4c-4h)

A mixture of 5-bromo-2-chloro-4-methyl-6-morpholinopyrimidine (**4**) (1g, 0.00342 mol), anhydrous potassium carbonate (1.42g, 0.0102 mol) and primary or secondary amines (0.00342 mol) in dry DMF was refluxed for about 8–10 h. Completion of the reaction was monitored by thin layer chromatography (TLC). The reaction mixture was cooled and poured in crushed ice. The resulting precipitate was filtered, washed with water, dried over reduced pressure and recrystallised from ethanol.

4.1.2.1. 9-(5-bromo-4-methyl-6-morpholinopyrimidin-2-yl)-9H-purine-2,6-diamine (**4a**)

White solid (90% yield); mp: 266-270°C; ¹H NMR (400 MHz, dmsO-d₆) δ 8.89 (s, 1H), 5.71 (s, 2H), 3.70 (bs 10H), 2.52 (s, 3H); ¹³C NMR (101 MHz, CDCl₃) δ 167.68, 164.10, 159.34, 156.08, 153.24, 150.22, 125.95, 115.28, 101.65, 65.98, 47.84, 25.38; LCMS: *m/z* 406.025.

4.1.2.2. 5-bromo-2-(1H-imidazol-1-yl)-4-methyl-6-morpholinopyrimidine (**4c**)

White solid (92% yield); mp: 96-100°C; ¹H NMR (400 MHz, CDCl₃) δ 8.53 (s, 1H), 7.77 (s, 1H), 7.10 (s, 1H), 3.83 (t, J= 8.1 Hz 4H), 3.67 (t, J= 7.8 Hz 4H), 2.57 (s, 3H); ¹³C NMR (101

MHz, CDCl₃) δ 168.57, 163.70, 151.57, 136.28, 130.42, 116.68, 103.94, 66.62, 48.94, 25.42;
GCMS: *m/z* 323.

4.1.2.3. 5-bromo-4-methyl-6-morpholino-N-(thiophen-2-ylmethyl)pyrimidin-2-amine (**4d**)

White solid (84% yield); mp: 106-110°C; ¹H NMR (400 MHz, CDCl₃) δ 7.34 (d, *J* = 7.9 Hz 1H), 6.28 (t, *J* = 8.2 Hz 1H), 6.14 (d, *J* = 7.8 Hz 1H), 4.79 (bs, 1H), 4.18 (d, *J* = 7.1 Hz, 2H), 3.71 – 3.67 (m, 4H), 3.43 – 3.38 (m, 4H), 2.46 (s, 3H); ¹³C NMR (101 MHz, CDCl₃) δ 168.93, 162.06, 159.36, 148.56, 146.83, 119.85, 114.72, 98.46, 66.37, 50.73, 44.45, 25.39;
GCMS: *m/z* 368

4.1.2.4. 2-((5-bromo-4-methyl-6-morpholinopyrimidin-2-yl)(methyl)amino)ethanol (**4e**)

White solid (78% yield); mp: 60-64°C; ¹H NMR (400 MHz, CDCl₃) δ 3.85-3.82 (m, 2H), 3.80 – 3.76 (m, 4H), 3.73 (bs 1H) 3.70 – 3.67 (m, 2H), 3.49 – 3.45 (m, 4H), 3.14 (s, 3H), 2.38 (s, 3H); ¹³C NMR (101 MHz, CDCl₃) δ 166.66, 163.19, 160.22, 95.40, 66.89, 63.44, 53.04, 48.70, 37.11, 25.43; GCMS: *m/z* 330

4.1.2.5. 1-(5-bromo-4-methyl-6-morpholinopyrimidin-2-yl)piperidine-4-carbonitrile (**4f**)

White solid (83% yield); mp: 87-91°C; ¹H NMR (400 MHz,) δ 3.86 (t, *J* = 7.6 Hz, 4H), 3.64 – 3.58 (m, 4H), 3.26 – 3.21 (m, 2H), 2.95-2.90 (m, 2H), 2.51- 2.46 (m, 1H), 2.26 (s, 3H), 1.74-1.70 (m, 2H), 1.43-1.37 (m, 2H); ¹³C NMR (101 MHz, CDCl₃) δ 167.83, 164.53, 162.56, 118.39, 96.73, 65.98, 45.37, 44.92, 43.08, 29.17, 25.33; GCMS: *m/z* 365

4.1.2.6. 1-(5-bromo-4-methyl-6-morpholinopyrimidin-2-yl)piperidine-4-carboxamide (**4g**)

White solid (88% yield); mp: 201-205°C; ¹H NMR (400 MHz, dms_o-d₆) δ 7.13 (s, 1H), 6.69 (s, 1H), 4.06 – 4.01 (m, 2H), 3.71 (t, *J* = 8.1 Hz, 4H), 3.53 – 3.48 (m, 4H), 3.02-2.98 (m, 2H), 2.78- 2.73 (m, 1H), 2.49 (s, 3H), 1.83-1.77 (m, 2H), 1.39-1.33 (m, 2H); ¹³C NMR (101 MHz, dms_o-d₆) δ 178.15, 166.18, 162.84, 160.93, 99.82, 67.29, 44.15, 43.27, 41.60, 27.73, 24.57; LCMS: *m/z* 384

4.1.2.7. N-(3-methoxyphenethyl)-5-bromo-4-methyl-6-morpholinopyrimidin-2-amine (**4h**)

White solid (91% yield); mp: 99-103°C; ¹H NMR (400 MHz, CDCl₃) δ 7.24 – 7.18 (m, 1H), 6.78 (m, 2H), 6.74 (s, 1H), 4.97 (bs, 1H), 3.81 – 3.77 (m, 7H), 3.59 (dt, *J* = 13.5, 6.9 Hz, 2H), 3.52 – 3.46 (m, 4H), 2.84 (t, *J* = 7.1 Hz, 2H), 2.39 (s, 3H); ¹³C NMR (101 MHz, CDCl₃) δ

166.91, 163.96, 159.82, 159.76, 141.00, 129.65, 121.24, 114.72, 111.62, 96.75, 66.96, 55.23, 49.05, 42.97, 36.08, 25.40; GCMS: *m/z* 406

4.1.3. Synthesis of 1-(5-bromo-4-methyl-6-morpholinopyrimidin-2-yl)-1H-indole (**4b**)

To a 0 °C solution of indole (0.4g, 0.00342 mol) in 10 mL of DMF was added sodium hydride (0.123g, 0.00513 mol, 60% dispersion in oil), stirred at 0°C for 30 min, then 5-bromo-2-chloro-4-methyl-6-morpholinopyrimidine (**4**) (1g, 0.00342 mol) was added, and the reaction mixture heated to 140°C for 2 h. The reaction mixture was cooled and diluted with water, the solid separated was filtered and recrystallised from alcohol.

White solid (75% yield); mp: 182-186°C; ¹H NMR (400 MHz, dms_o-d₆) δ 8.62 (d, *J* = 8.2 Hz, 1H), 8.17 (d, *J* = 3.0 Hz, 1H), 7.59 (d, *J* = 7.6 Hz, 1H), 7.28 (t, *J* = 7.7 Hz, 1H), 7.17 (t, *J* = 7.2 Hz, 1H), 6.71 (d, *J* = 2.9 Hz, 1H), 3.75 (s, 4H), 3.61 (s, 4H), 2.56 (s, 3H); ¹³C NMR (101 MHz, dms_o-d₆); 168.31, 163.24, 158.99, 143.43, 130.68, 125.05, 123.89, 121.72, 114.09, 112.33, 101.21 98.73, 66.86, 49.69, 25.33; GCMS: *m/z* 372

4.1.4. General procedure for synthesis of (**5a & 5c-5h**)

A mixture of 2-chloro-4-methyl-6-morpholinopyrimidine (**3**) (1g, 0.00469 mol), anhydrous potassium carbonate (1.94g, 0.0141 mol) and primary or secondary amines (0.00469 mol) in dry DMF was refluxed for about 8–10 h. Completion of the reaction was monitored by thin layer chromatography (TLC). The reaction mixture was cooled and poured in crushed ice. The resulting precipitate was filtered, washed with water, dried over reduced pressure and recrystallised from ethanol.

4.1.4.1. 9-(4-methyl-6-morpholinopyrimidin-2-yl)-9H-purine-2,6-diamine (**5a**)

White solid (89% yield); mp: 248-252°C; ¹H NMR (400 MHz, dms_o-d₆) δ 8.94 (s, 1H), 5.91 (s, 1H), 5.68 (bs, 2H), 3.78-3.72 (m 4H), 3.60-3.55 (m, 6H), 2.49 (s, 3H); ¹³C NMR (101 MHz, CDCl₃) δ 167.32, 163.95, 158.78, 156.47, 152.89, 149.71, 124.08, 115.20, 100.16, 66.05, 48.48, 25.49; GCMS: *m/z* 327

4.1.4.2. 2-(1H-imidazol-1-yl)-4-methyl-6-morpholinopyrimidine (**5c**)

White solid (91% yield); mp: 70-74°C; ¹H NMR (400 MHz, CDCl₃) δ 8.50 (s, 1H), 7.80 (s, 1H), 7.07 (s, 1H), 6.20 (s, 1H), 3.80 – 3.76 (m, 4H), 3.64 (t, *J* = 6.6 Hz, 4H), 2.36 (s, 3H). ;

^{13}C NMR (101 MHz,) δ 167.57, 163.23, 154.27, 136.28, 129.74, 116.73, 99.05, 66.41, 44.38, 24.27.; GCMS: m/z 245

4.1.4.3. 4-methyl-6-morpholino-N-(thiophen-2-ylmethyl)pyrimidin-2-amine (5d)

White solid (82% yield); mp: 97-101°C; ^1H NMR (400 MHz, CDCl_3) δ 7.43 (d, $J = 8.2$ Hz 1H), 6.31 (t, $J = 8.0$ Hz 1H), 6.18 (d, $J = 7.8$ Hz 1H), 5.96 (s, 1H), 4.63 (bs, 1H), 4.11 (d, $J = 8.1$ Hz, 2H), 3.76 – 3.71 (m, 4H), 3.48 – 3.43 (m, 4H), 2.51 (s, 3H); ^{13}C NMR (101 MHz, CDCl_3) δ 167.08, 162.12, 159.96, 149.84, 146.27, 120.35, 114.48, 97.73, 66.66, 51.55, 45.03, 25.47; GCMS: m/z 290

4.1.4.4. 2-(methyl(4-methyl-6-morpholinopyrimidin-2-yl)amino)ethanol (5e)

White solid (79% yield); mp: 58-62°C; ^1H NMR (400 MHz, CDCl_3) δ 6.14 (s, 1H) 3.83-3.75 (m, 6H), 3.70 (bs 1H) 3.62– 3.58 (m, 2H), 3.50 – 3.46 (m, 4H), 3.46 (s, 3H), 2.42 (s, 3H); ^{13}C NMR (101 MHz, CDCl_3) δ 167.11, 163.65, 161.75, 97.40, 66.36, 62.98, 53.56, 47.87, 37.69, 25.40; GCMS: m/z 252

4.1.4.5. 1-(4-methyl-6-morpholinopyrimidin-2-yl)piperidine-4-carbonitrile (5f)

White solid (80% yield); mp: 75-79°C; ^1H NMR (400 MHz,) δ 6.01 (s, 1H), 3.80-075 (m, 4H), 3.53 (t, $J = 7.6$ Hz, 4H), 3.16 – 3.12 (m, 2H), 2.90-2.86 (m, 2H), 2.59- 2.53 (m, 1H), 2.37 (s, 3H), 1.79-1.75 (m, 2H), 1.42-1.38 (m, 2H); ^{13}C NMR (101 MHz, CDCl_3) δ 166.48, 163.93, 162.24, 120.02, 98.04, 66.05, 45.68, 44.91, 43.10, 29.06, 25.39; GCMS: m/z 287

4.1.4.6. 1-(4-methyl-6-morpholinopyrimidin-2-yl)piperidine-4-carboxamide (5g)

White solid (90% yield); mp: 187-191°C; ^1H NMR (400 MHz,) δ 7.24 (s, 1H), 6.74 (s, 1H), 5.91 (s, 1H), 4.56- 4.60 (m, 2H), 3.61 – 3.56 (m, 4H), 3.46 – 3.40 (m, 4H), 2.69 (td, $J = 12.8$, 2.1 Hz, 2H), 2.26 (tt, $J = 11.6$, 3.6 Hz, 1H), 2.08 (s, 3H), 1.65 (qd, $J = 12.7$, 2.2 Hz, 2H), 1.36 (qd, $J = 12.5$, 4.0 Hz, 2H). ; ^{13}C NMR (101 MHz,) δ 177.07, 166.28, 163.54, 161.52, 91.84, 66.38, 44.37, 43.52, 42.62, 28.84, 24.69; GCMS: m/z 305

4.1.4.7. N-(3-methoxyphenethyl)-4-methyl-6-morpholinopyrimidin-2-amine (5h)

White solid (88% yield); mp: 96-100°C; ^1H NMR (400 MHz, CDCl_3) δ 7.29 (t, $J = 7.7$ Hz 1H), 6.89 (d, $J = 7.9$ Hz 1H), 6.80 (d, $J = 8.0$ Hz 1H), 6.71 (s, 1H), 5.91 (s, 1H) 4.65 (bs, 1H), 3.76 – 3.71 (m, 4H) 3.65 (s, 3H), 3.58-3.53 (m, 2H), 3.48 – 3.43 (m, 4H), 2.82 (t, $J = 7.8$ Hz, 2H), 2.46 (s, 3H); ^{13}C NMR (101 MHz, CDCl_3) δ 167.36, 164.71, 160.22, 159.80,

141.48, 129.94, 121.61, 115.28, 112.86, 98.34, 66.36, 55.04, 48.25, 42.47, 35.79, 25.49;
GCMS: *m/z* 328

4.1.5. Synthesis of 1-(4-methyl-6-morpholinopyrimidin-2-yl)-1H-indole (**5b**)

To a 0 °C solution of indole (0.55g, 0.00469 mol) in 10 mL of DMF was added sodium hydride (0.169g, 0.0070 mol, 60% dispersion in oil), stirred at 0°C for 30 min, then 5-bromo-2-chloro-4-methyl-6-morpholinopyrimidine (**3**) (1g, 0.00469 mol) was added, and the reaction mixture heated to 140°C for 2 h. The reaction mixture was cooled and diluted with water, the solid separated was filtered and recrystallised from alcohol.

White solid (72% yield); mp: 176-180°C; ¹H NMR (400 MHz, dms_o-d₆) δ 8.48 (d, *J* = 8.0 Hz, 1H), 8.13 (s, 1H), 7.48 (d, *J* = 7.4 Hz, 1H), 7.31 (t, *J* = 8 Hz, 1H), 7.14 (t, *J* = 7.6 Hz, 1H), 6.79 (t, *J* = 8 Hz 1H), 6.18 (s, 1H), 3.75 (s, 4H), 3.61 (s, 4H), 2.56 (s, 3H); ¹³C NMR (101 MHz, dms_o-d₆); 167.93, 164.04, 159.07, 143.65, 131.74, 129.05, 124.46, 122.68, 113.98, 112.79, 102.52, 99.13, 67.17, 49.82, 26.02; GCMS: *m/z* 294

4.2. In vitro Anticancer activity

4.2.1. Cell lines and culture conditions.

HeLa (cervix), NCI-H460 (lung), MCF-7(breast), HepG2 (liver) and IMR-32 (brain) cell lines were purchased from National Centre for Cell Science, Pune, India. Cells were cultured in MEM and RPMI-1640 containing 10% FBS, 100 U of Penicillin G/ml and 100 µg/ml of streptomycin at 37 °C in a humidified atmosphere containing 5% CO₂.

4.2.2. Assessment of cell viability and morphology.

Effect of 4-methyl-6-morpholinopyrimidine derivatives on viability of HeLa and NCI-H460 cells was assessed using 3-(4, 5-dimethylthiazol-2-yl)-2, 5-diphenyl tetrazolium bromide (MTT) assay. Sub-confluent, HeLa, NCI-H460, MCF-7, HepG2 and IMR-32 were seeded at 5 × 10⁴ cells/ml in 96 well plates for 24 h. Cells were then treated with increasing concentrations (5, 10 and 20 µM) of compounds for 24 h. DMSO treated cells were used as the vehicle control. Following treatment, 10 µl of MTT (5 mg/ml) was added to each well followed by lysis of the cells using 100 µl of 10% SDS in 0.01 N HCl and absorbance was measured at 570 nm, with reference wavelength of 640 nm, using Tecan i-200 microplate reader. Percent viability was calculated by considering vehicle control as 100%. In another

experiment, HeLa and NCI-H460 cells were treated as mentioned above and the cellular morphological changes were photographed using phase contrast microscope.

4.2.3. Cell cycle analysis.

The distribution of HeLa and NCI-H460 cells in different phases of cell-cycle after treatment with **4c** and **5h** compounds respectively was determined by flow cytometry. Briefly, 0.1×10^6 cells were cultured in 12 well plate and treated with different concentration (5, 10 and 20 μM) of compounds for 24 h. Post treatment cells were harvested, washed and fixed in 70% chilled ethanol. Cells were then rehydrated in PBS (phosphate buffer saline) and RNA was hydrolysed using 50 μl of Ribonuclease A (5 mg/ml in PBS, DNase free) for overnight at room temperature. DNA was stained with Propidium Iodide (50 μM in PBS) for 30 min at 37°C and DNA content was analyzed on the FL-2A channel of Flow Cytometer (FACS Calibur, BD) equipped with a 488nm argon laser. The data was analyzed by Cell Quest Pro software (BD) for the distribution of cells in different phases of cell cycle.

4.2.4. Detection of Apoptosis by Annexin-V/PI staining.

HeLa and NCI-H460 cells (0.1×10^6) cultured in 12 well plates were treated with or without **4c** and **5h** compounds respectively for 24 h. cells were then harvested by gentle trypsinization, washed with PBS and resuspended in binding buffer from BD Annexin-V kit. Cells were then incubated with 5 μl FITC Annexin-V and 5 μl of PI (Propidium Iodide) for 5 min at 37°C in the dark before analysis by flow cytometry (FACS Calibur, BD). The percentages of cells positive for Annexin V, PI alone and both Annexin V and PI were calculated by dot blot analysis using Cell Quest Pro software (BD Biosciences).

4.2.5. Analysis of mitochondrial membrane potential.

Alterations in mitochondrial membrane potential were determined using cytofluorimetric, lipophilic cationic dye, 5,5',6,6'-tetrachloro-1,1',3,3'- tetraethylbenzimidazolylcarbocyanine iodide (JC-1). HeLa and NCI-H460 cells (0.1×10^6) were treated with or without **4c** and **5h** compounds respectively at different concentrations (5, 10 and 20 μM) for 24 h. Following treatment cells were harvested, washed with PBS and resuspend in 1 ml of freshly prepared 2.5 μM JC-1 solution followed by incubation at 37°C for 20 min. Cells were analyzed by flow cytometry (FACS Calibur, BD) with an excitation of 488 nm and emission of 530 nm.

4.2.6. Detection of intracellular Reactive Oxygen Species generation.

Intracellular ROS production was determined using cell permeable fluorescent probe 2, 7-dichlorodihydro fluorescein diacetate (DCFDA-H2). Briefly, HeLa and NCI-H460 cells were treated with **4c** and **5h** (10 μ M) for 24h. After treatment, cells were washed with PBS and stained with 15 μ M DCFDA-H2 for 10 min at 30 °C. The relative fluorescence intensity was analysed using fluorescence microscopy.

4.2.7. Determination of Caspase 3/7 activity.

Activation of Caspase-3/7 was measured in order to determine induction of apoptosis, as per the manufacturer's protocol supplied in caspase-activity detection kit (Promega). HeLa and NCI-H460 cells (10 $\times 10^4$ cells/ml) were cultured in 96 well plates and treatment was carried out according to previously mentioned protocol for cell viability assay. Cell apoptosis was then determined by measuring caspase-3/7 activity using Caspase Glo-3/7 assay.

4.2.8. Nuclear morphological changes.

Changes in nuclear morphology of cells treated with compound **4c** and **5h** was determined by staining with DAPI (4',6-Diamidino-2-Phenylindole). Briefly, cells were treated with **4c** and **5h** compounds for 24 h, washed with PBS and fixed with 2% neutral buffered formalin solution for 10 min. Cell permeabilization was carried out using 0.2% triton-x for 5min, followed by staining with DAPI (1 mg/mL) for 10 min. Cells were examined for morphological changes under fluorescence microscope.

4.2.9. Statistical analysis.

Experiments were performed in multiple sets and results were analyzed for statistical significance, using One-way ANOVA followed by Tukey's multiple comparison tests utilizing GraphPad Prism5 software; *P*-values are mentioned in figure legends.

4.3. DNA fragmentation assay.

The fragmentation of DNA after treatment with compounds was determined using agarose gel electrophoresis. Briefly, HeLa and NCI-H460 cells were treated with and without **4c** and **5h** respectively at different concentrations (5, 10 and 20 μ M) for 24 h. Cells were harvested and total genomic DNA was isolated using standard protocol. The fragmentation of DNA was determined by resolving DNA on 2% agarose gel. Standard DNA marker was used to compare the fragmentation.

4.4. Molecular modelling studies.

The modelling of the catalytic domain of the mTOR was done as described earlier [1]. Sequence of mTOR (IDP42345) was obtained from uniprot (www.uniprot.org), and as the mTOR catalytic domain is localized between amino acids 2181 and 2516, the same was used for homology modelling using the Swiss-Model server (<http://swissmodel.expasy.org/>) using the mTOR Cryo-EM structure (5H64) available in PDB database (www.rcsb.org/). The mTOR model was then prepared for docking using UCSF Chimera package [2], where hydrogens were added and Gasteiger charges were computed. The small molecules, **4c** and **5h** were drawn in Marvin Sketch program (Chem Axon), and further processed with Swissparam (www.swissparam.ch/), which provide topology and parameter for small organic molecules. The docking analysis of the small molecules on the catalytic domain of the mTOR was performed using Autodock Vina (Trott and Olson 2010) The docked structures were analysed by DSV studio viewer (Accelrys Software Inc.) for determining the ligand interactions.

Acknowledgements

The authors gratefully acknowledge the financial assistance from Department of Science & Technology (DST-SERB), Govt. of India, New Delhi under Major Research Project No. SR/S1/OC-58/2011 and University Grant Commission (UGC), New Delhi under UPE-FAR-I program, F. No. 14-3/2012 (NS/PE) and we are also grateful to the University Scientific Instrumentation Centre (USIC), Karnatak University, Dharwad for Spectral Analysis. One of the authors Supreet Gaonkar is thankful to UGC, New Delhi, for providing Senior Research Fellowship (SRF).

Conflict of interest

None declared

Reference

1. WHO, Cancer, World Health Organization 2015.
2. D. Hanahan and R. A. Weinberg, *Cell*, 2011, **144**, 646-674.
3. V. V. Padma *BioMedicine* 2015, **5**, 1-6.
4. E. Vitaku, D. T. Smith and J. T. Njardarson, *J. Med. Chem.*, 2014, **57**, 10257–10274.
5. P. C. Diao, Q. Li, M. J. Hu, Y. F. Ma, W. W. You, K. H. Hong and P. Li. Zhao, *Eur. J. Med. Chem.*, 2017, **134**, 110-118.

6. O. Phuangsawai, P. Beswick, S. Ratanabunyong, L. Tabtimmai, P. Suphakun, P. Obounchoey, P. Srisook, N. Horata, I. Chuckowree, S. Hannongbua, S. E. Ward, K. Choowongkomon and M. P. Gleeson, *Eur. J. Med. Chem.*, 2016, **124**, 896-905.
7. M. Krecmerova, M. Dracinsky, R. Snoeck, J. Balzarini, K. Pomeisl and G. Andrei, *Bioorg. Med. Chem.*, 2017, **25**, 4637-4648.
8. S. M. Roopan and R. Sompalle, *Synth. Commun.* 2016, **46**, 645-672.
9. T. Gregoric, M. Sedic, P. Grbic, A. T. Paravic, S. K. Pavelic, M. Cetina, R. Vianello and S Raic-Malic, *Eur. J. Med. Chem.*, 2017, **125**, 1247-1267.
10. J. Boyer, E. Arnoult, M. Medebielle, J. Guillemont, J. Unge and D. Jochmans, *J. Med. Chem.*, 2011, **54**, 7974-7985.
11. J. Cieplik, M. Stolarczyk, J. Pluta, O. Gubrynowicz, I. Bryndal, T. Lis and M. Mikulewicz, *Acta. Pol. Pharm.*, 2011, **68**, 57-65.
12. O. Alam, S. A. Khan, N. Siddiqui, W. Ahsan, S. P. Verma and S. J. Gilani, *Eur. J. Med. Chem.*, 2010, **45**, 5113-5119.
13. O. Alam, P. Mullick, S. P. Verma, S. J. Gilani, S. A. Khan, N. Siddiqui and W. Ahsan, *Eur. J. Med. Chem.*, 2010, **45**, 2467-2472.
14. J. D. Bhatt, C. J. Chudasama and K. D. Patel, *Bioorg. Med. Chem.*, 23 (2015), **23**, 7711-7716.
15. V. Alagarsamy, S. Meena, K.V. Ramseshu, V.R. Solomon, K. Thirumurugan, K. Dhanabal and M. Murugan, *Eur. J. Med. Chem.*, 2006, **41**, 1293-1300.
16. K. Singh and T. Kaurb, *Med. Chem. Commun.*, 2016, **7**, 749-768.
17. V. Pal'chikov, *Russ. J. Org. Chem.* 2013, **49**, 787-814.
18. W. Peng, Z. C. Tu, Z. J. Long, Q. Liu and G. Lu, *Eur. J. Med. Chem.*, 2016, **108**, 644-654.
19. V. Kanagarajan, J. Thanusu and M. Gopalakrishnan, *Eur. J. Med. Chem.*, 2010, **45**, 1583-1589.
20. Y. Wada, R. Lu, D. Zhou, J. Chu, T. Przewloka, S. Zhang, L. Li, Y. Wu, J. Qin, V. Balasubramanyam, J. Barsoum and M. Ono, *Blood*, 2007, **109**, 1156-1164
21. V. Samano, V. L. Styles and J. H. Chan, *J. Heterocyc. Chem.*, 2000, **37**, 183-185.
22. K. Singh, H. Kaur, P. Smith, C. de Kock, K. Chibale and J. Balzarini, *J. Med. Chem.*, 2014, **57**, 435-448.
23. C. M. Dehnhardt, A. M. Venkatesan, E. D. Santos, Z. Chen, O. Santos, S. A. Kaloustian, N. Brooijmans, R. Mallon, I. Hollander, L. Feldberg, J. Lucas, I. Chaudhary, K. Yu, J. Gibbons, R. Abraham and T. S. Mansour, *J. Med. Chem.*, 2010, **53**, 798-810.

24. K. M. Foote, K. Blades, A. Cronin, S. Fillery, S. S. Guichard, L. Hassall, I. Hickson, X. Jacq, P. J. Jewsbury, T. M. McGuire, J. W. M. Nissink, R. Odedra, K. Page, P. Perkins, A. Suleman, K. Tam, P. Thommes, R. Broadhurst and C. Wood, Discovery of 4-[(3R)-3-Methylmorpholin-4-yl]-6-[1-(methylsulfonyl)cyclopropyl]pyrimidin-2-yl} 1H-indole, *J. Med. Chem.*, 2013, **56**, 2125–2138.
25. V. Asati, D. K. Mahapatra and S. K. Bharti, *Eur. J. Med. Chem.*, 2016, **109**, 314–341.
26. D. P. Sutherland, L. Bao, M. Berry, G. Castanedo, I. Chuckowree, J. Dotson, A. Folks, L. Friedman, R. Goldsmith, J. Gunzner, T. Heffron, J. Lesnick, C. Lewis, S. Mathieu, J. Murray, J. Nonomiya, J. Pang, N. Pegg, W. W. Prior, L. Rouge, L. Salphati, D. Sampath, Q. Tian, V. Tsui, N. C. Wan, S. Wang, B. Wei, C. Wiesmann, P. Wu, B.-Y. Zhu and A. Olivero, *J. Med. Chem.*, 2011, **54**, 7579–7587.
27. A. J. Folkes, K. Ahmadi, W. K. Alderton, S. Alix, S. J. Baker, G. Box, I. S. Chuckowree, P. A. Clarke, P. Depledge, S. A. Eccles, L. S. Friedman, A. Hayes, T. C. Hancox, A. Kugendradas, L. Lensun, P. Moore, A. G. Olivero, J. Pang, S. Patel, G. H. Pergl-Wilson, F. I Raynaud, A. Robson, N. Saghir, L. Salphati, S. Sohal, M. H. Ultsch, M. Valenti, H. J. A. Wallweber, N. C. Wan, C. Wiesmann, P. Workman, P. Zhyvoloup, M. J. Zvelebil and S. J. Shuttleworth, *J. Med. Chem.*, 2008, **51**, 5522–5532.
28. S. Park, N. Chapuis, V. Bardet, J. Tamburini, N. Gallay, L. Willems, Z.A. Knight, K.M. Shokat, N. Azar, F. Viguie, N. Ifrah, F. Dreyfus, P. Mayeux, C. Lacombe and D. Bouscary, *Leukemia*, 2008, **22**, 1698–1706.
29. T. P. Heffron, M. Berry, G. Castanedo, C. Chang, I. Chuckowree, J. Dotson, A. Folkes, J. Gunzner, J. D. Lesnick, C. Lewis, S. Mathieu, J. Nonomiya, A. Olivero, J. Pang, D. Peterson, L. Salphati, D. Sampath, S. Sideris, D. P. Sutherland, V. Tsui, N. C. Wan, S. Wang, S. Wong and B.-Y. Zhu, *Bioorg. Med. Chem. Lett.*, 2010, **20**, 2408–2411.
30. O. V. Dolomanov, L. J. Bourhis, R. J. Gildea, J. A. K. Howard and H. Puschmann, *J. Appl. Cryst.*, 2009, **22**, 339–341.
31. G. M. Sheldrick, *Acta Cryst.* 2008, **A64**, 112–122.
32. I. Ali, M. N. Lonea and H. Y. Aboul-Eneinb, *Med. Chem. Commun.*, 2017, **8**, 1742–1773.
33. V. Pomel, P. Gaillard, G. Desforges, A. Quattropani and C. Montagne, WO Pat., 2010037765 A2, 2010.
34. M. A. Musa, V. L. D. Badisa and L. M. Latinwo, *Anticancer Res.*, 2014, **34**, 1601–1608.
35. G. K. Schwartz and M. A. Shah, *J. Clin. Oncol.*, 2005, **23**, 9408–9421.
36. N. P. Kumar, P. Sharma, T. S. Reddy, S. Nekkanti, N. Shankaraiah, G. Lalita, S.

- Sujanakumari, S. K. Bhargava, V.G.M. Naidu and A. Kamal, *Eur. J. Med. Chem.*, 2017, **127**, 305-317
37. A. Nagarsenkar, L. Guntuku, S. D. Guggilapu, K. Danthi Bai, S. Gannoju, V.G.M. Naidu and N. B. Bathini, *Eur. J. Med. Chem.*, 2016, **124**, 782-793.
38. M. Kajstura, H. D. Halicka, J. Pryjma and Z. Darzynkiewicz, *Cytometry Part A*, 2007, **71A**, 125–131.
39. X. Huang, H. D. Halicka, F. Traganos, T. Tanaka, A. Kurose and Z. Darzynkiewicz, *Cell Prolif.*, 2005, **38**, 223–243.
40. P. A. Leventis and S. Grinstein, *Annu. Rev. Biophys.*, 2010, **39**, 407–427.
41. V. E. Kagan, J. P. Fabisiak, A. A. Shvedova, Y.Y. Tyurina, V. A. Tyurin, N. F. Schor and K. Kawai, *FEBS Lett.*, 2000, **477**, 1-7
42. M. Engeland, L. J. W. Nieland, F. C. S. Ramaekers, B. Schutte and C. P. M. Reutelingsperger, *Cytometry*, 1998, **31**, 1-9.
43. S. H. Lee, X. W. Meng, K. S. Flatten, D. A. Loegering and S. H. Kaufmann, *Cell Death Differ.*, 2013, **20**, 64–76
44. H. U. Simon, A. Haj-Yehia and F. Levi-Schaffer, *Apoptosis*, 2000, **5**, 415-418.
45. F. Sesti, O. E. Tsitsilonis, A. Kotsinas and I. P. Trougakos, *in vivo*, 2012, **26**, 395-402.
46. D. Trachootham, J. Alexandre and P. Huang, *Nat. Rev. Drug Discov.*, 2009, **8**, 579-591.
47. Y. Zou, C. Yan, H. Zhang, J. Xu, D. Zhang, Z. Huang and Y. Zhang, *Eur.J. Med. Chem.*, 2017, **138**, 313-319.
48. Y. Zheng, L. Zhu, L. Fan, W. Zhao, J. Wang, X. Hao, Y. Zhu, X. Hu, Y. Yuan, J. Shao and W. Wang, *Eur. J. Med. Chem.*, 2017, **125**, 902-913.
49. L. A. Sena and N. S. Chandel, *Mol. Cell.*, 2012, **48**, 158–167.
50. S. Maharjan, M. Oku, M. Tsuda, J. Hoseki and Y. Sakai, *Sci. Rep.*, 2014, **4**, 1-11.
51. A. Cossarizza, M. Baccaranicontri, G. Kalashnikova and C. Franceschi, *Biochem. Biophys. Res. Commun.*, 1993, **197**, 40-45
52. M. Higuchi, T. Honda, R. J. Proske and E. T. Yeh, *Oncogene*, 1998, **17**, 2753-2760
53. J. M. Mates and F. M. Sanchez-Jimenez, *Int. J. Biochem. Cell Biol.*, 2000, **32**, 157-170
54. S. Kawanishi and Y. Hiraku, *Curr. Med. Chem.- Anticancer Agents.*, 2004, **4**, 415-9.
55. H. Mizutani, S. Tada-Oikawa, Y. Hiraku, M. Kojima and S. Kawanishi, *Life Sci.*, 2005, **76**, 1439–1453.
56. K. Tanneeru, B. M. Reddy and L. Guruprasad, *Med. Chem. Res.*, 2012, **21**, 1207-1217.
57. O. Trott, and A. J. Olson, *J. Comput. Chem.*, 2010, **31**, 455-461.

58. J. C. Verheijen, D. J. Richard, K. Curran, J. Kaplan, M. Lefever, P. Nowak, D. J. Malwitz, N. Brooijmans, L. Toral-Barza, W.-G. Zhang, J. Lucas, I. Hollander, S. Ayril-Kaloustian, T. S. Mansour, K. Yu and A. Zask, *J. Med. Chem.*, 2009, **52**, 8010–8024.

Figure Legends

Figure 1: Examples of PI3K/mTOR inhibitors.

Figure 2: ORTEP diagram of compound **4h** with labeling showing 50% displacement ellipsoids (Crystal structure drew in Mercury 3.7)

Figure 3: Packing diagram of **4h** with Br...Br(3.590 Å) Br... π (3.491 Å) and also CH... π (2.892 Å) interactions

Figure 4: Dose-dependent effect of **4c** (**A**) and **5h** (**B**) compounds on human cancer HeLa and NCI-H460 cell proliferation. Results of MTT assay are represented as percentage of cell viability at different concentrations of **4c** and **5h**, where error bars represents SEM of triplicate determinations from three different assessments. *** $p > 0.001$. The cellular morphology of HeLa and NCI-H460 cells after treatment with or without **4c** and **5h** compounds was analysed and photographed using phase contrast microscope (**C**).

Figure 5: Effect of **4c** and **5h** compounds on cell cycle progression of cancer cells. Histograms represent distribution of HeLa and NCI-H460 cells in different phases of cell cycle after treatment with or without **4c** and **5h** compounds, respectively at different concentrations (0-20 μ M) (**A**). Bar graph indicates percentage of HeLa and NCI-H460 cell population after treatment with or without **4c** and **5h** compounds, respectively in subG1, G1, S, and G2–M phases of the cell cycle (**B & C**).

Figure 6: Morpholino pyrimidine compounds induce cell apoptosis. Histograms represent distribution of HeLa and NCI-H460 cells in different phases Q1 (necrotic/dead cells), Q2 (late apoptosis cells), Q3 (live cells) and Q4 (early apoptosis cells) after treatment with or without 4c and 5h compounds, respectively at different concentrations (0-20 μ M) (A). Bar graph indicates percentage of HeLa and NCI-H460 cell population in Q1, Q2, Q3 and Q4 phases after treatment with or without 4c and 5h compounds, respectively (B & C).

Figure 7: Loss of mitochondrial membrane potential induced by Morpholino pyrimidine compounds. Density plot representing JC-1-stained HeLa and NCI-H460 cells after treatment with different concentrations (0-20 μ M) of 4c and 5h compounds, respectively. P1 represents population of cells with low mitochondrial membrane potential emitting green fluorescence (A). Bar graph represents percentage of high mitochondrial membrane potential cells emitting red fluorescent (P2) against low mitochondrial membrane potential cells emitting green fluorescence (P1) (B & C).

Figure 8: Morpholino pyrimidine compounds induced apoptosis is associated with ROS production, activation of caspases, chromatin condensation and DNA fragmentation. Intracellular ROS production in HeLa and NCI-H460 cells after treatment with 4c and 5h compounds respectively was determined by fluorescence microscopy using ROS specific fluorescent probe (DCFDA-H2) (A). Activation of executioner caspases (caspase3/7) in HeLa and NCI-H460 cells after treatment with 4c and 5h compounds respectively was determined by measuring caspase 3/7 activity using caspase 3/7 Glo assay and represented as fold increase in activity ***P>0.001 (B). Agarose gel profiles showing DNA fragmentation in HeLa and NCI-H460 cells after treatment with 4c and 5h compounds respectively at different concentrations (0-20 μ M) (C). DAPI-staining showing the chromatin-condensed nuclei in apoptotic cells following treatment with 4c and 5h compounds. (D). ‘‘M’’ is marker

Figure 9: Docking analysis of 4c and 5h shows the binding of these molecules at the binding domain of the mTOR molecule. 4C at the binding domain of the mTOR shows interactions with the neighbouring amino acids (A). Surface around the 4c molecule interacting with the mTOR molecule (B). 5h at the binding domain of the mTOR showing interactions with the neighbouring amino acids (C). Surface around the 5h molecule interacting with the mTOR molecule (D).

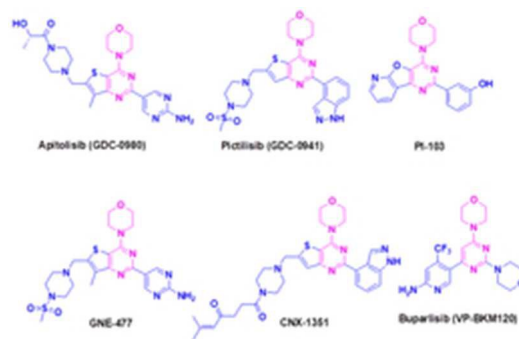


Figure 1: Examples of PI3K/mTOR inhibitors.

22x14mm (300 x 300 DPI)

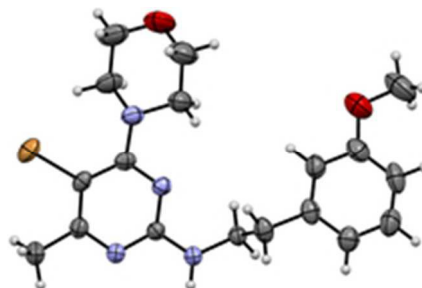


Figure 2: ORTEP diagram of compound 4h with labeling showing 50% displacement ellipsoids (Crystal structure drew in Mercury 3.7)

18x12mm (300 x 300 DPI)

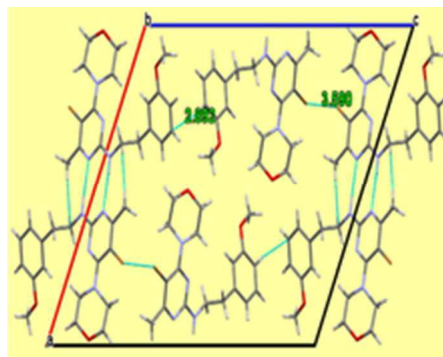


Figure 3: Packing diagram of 4h with Br...Br(3.590 Å) Br...n (3.491 Å) and also CH... n (2.892 Å) interactions

18x14mm (300 x 300 DPI)

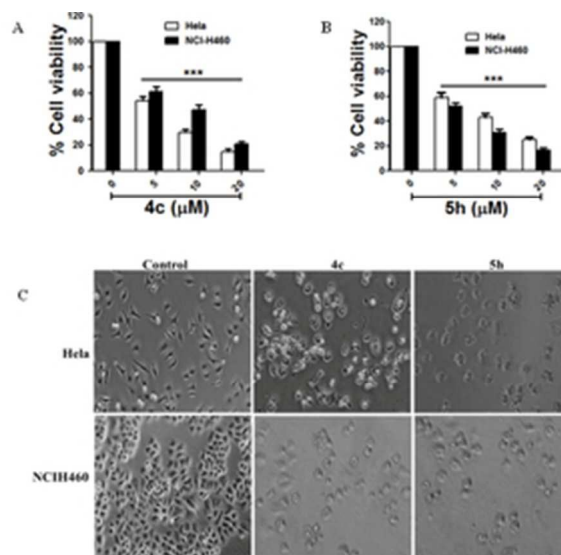


Figure 4: Dose-dependent effect of 4c (A) and 5h (B) compounds on human cancer HeLa and NCI-H460 cell proliferation. Results of MTT assay are represented as percentage of cell viability at different concentrations of 4c and 5h, where error bars represents SEM of triplicate determinations from three different assessments. *** $p > 0.001$. The cellular morphology of HeLa and NCI-H460 cells after treatment with or without 4c and 5h compounds was analysed and photographed using phase contrast microscope (C).

24x23mm (300 x 300 DPI)

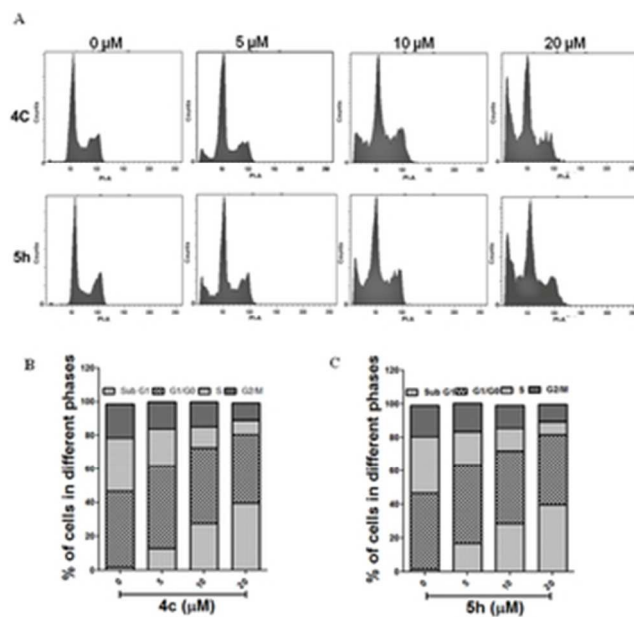


Figure 5: Effect of 4c and 5h compounds on cell cycle progression of cancer cells. Histograms represent distribution of HeLa and NCI-H460 cells in different phases of cell cycle after treatment with or without 4c and 5h compounds, respectively at different concentrations (0–20 μM) (A). Bar graph indicates percentage of HeLa and NCI-H460 cell population after treatment with or without 4c and 5h compounds, respectively in subG1, G1, S, and G2–M phases of the cell cycle (B & C).

27x25mm (300 x 300 DPI)

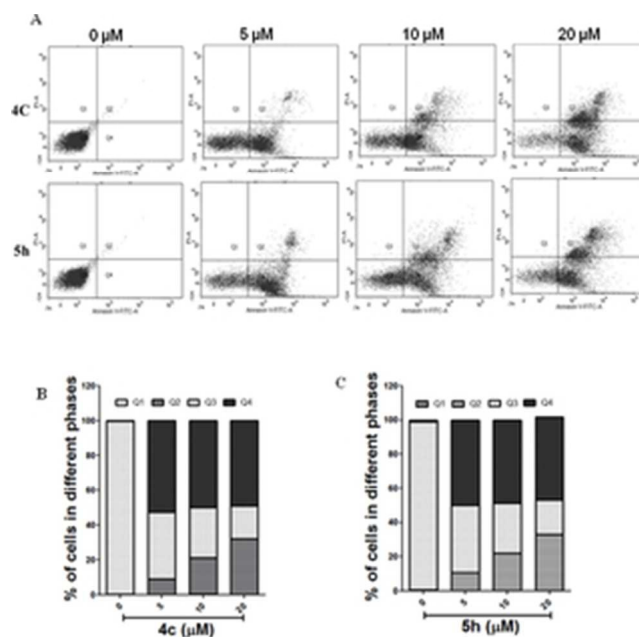


Figure 6: Morpholino pyrimidine compounds induce cell apoptosis. Histograms represent distribution of HeLa and NCI-H460 cells in different phases Q1 (necrotic/dead cells), Q2 (late apoptosis cells), Q3 (live cells) and Q4 (early apoptosis cells) after treatment with or without 4c and 5h compounds, respectively at different concentrations (0-20μM) (A). Bar graph indicates percentage of HeLa and NCI-H460 cell population in Q1, Q2, Q3 and Q4 phases after treatment with or without 4c and 5h compounds, respectively (B & C).

27x26mm (300 x 300 DPI)

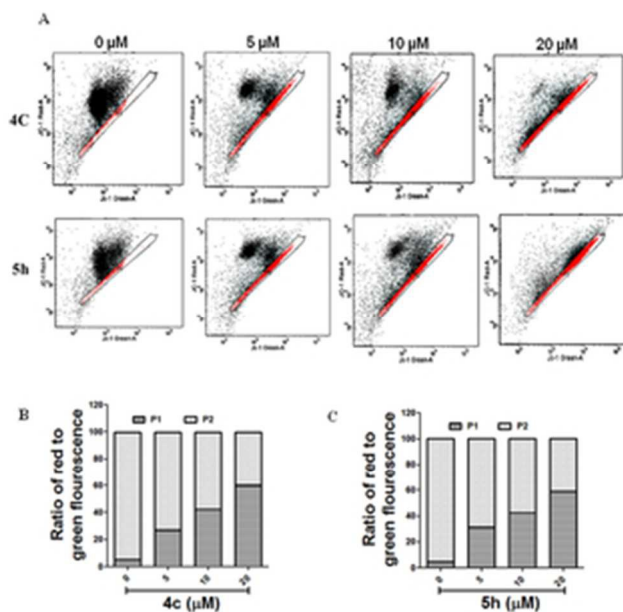


Figure 7: Loss of mitochondrial membrane potential induced by Morpholino pyrimidine compounds. Density plot representing JC-1-stained HeLa and NCI-H460 cells after treatment with different concentrations (0-20 μM) of 4c and 5h compounds, respectively. P1 represents population of cells with low mitochondrial membrane potential emitting green fluorescence (A). Bar graph represents percentage of high mitochondrial membrane potential cells emitting red fluorescent (P2) against low mitochondrial membrane potential cells emitting red fluorescence (P1) (B & C).

27x25mm (300 x 300 DPI)

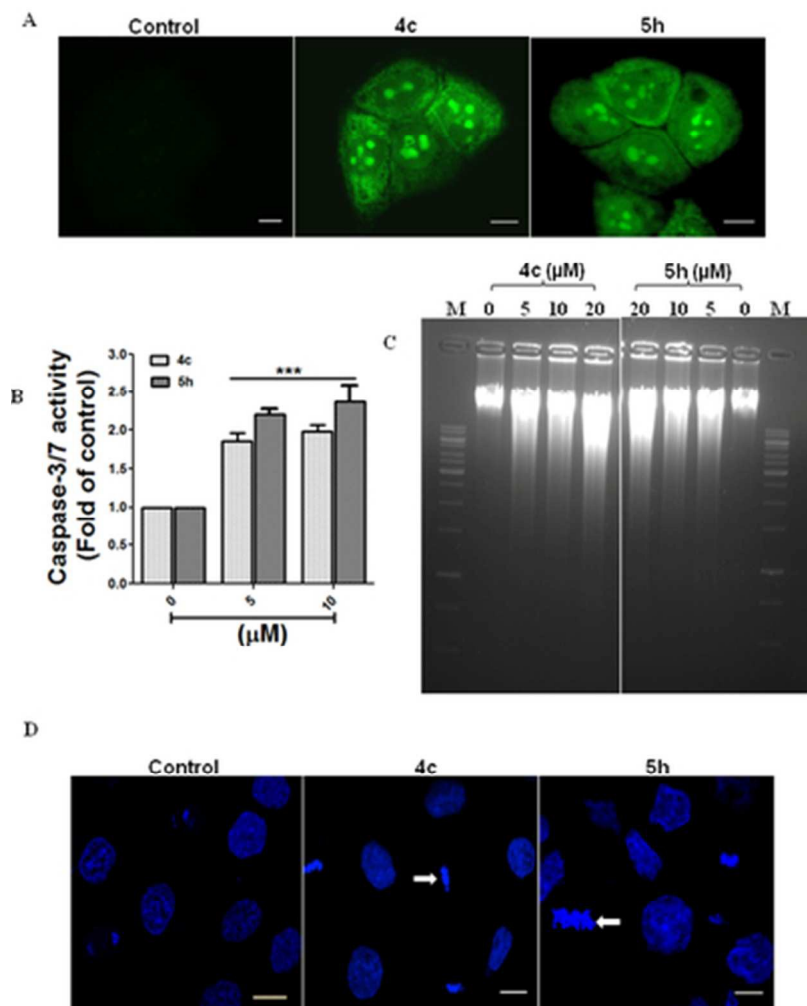


Figure 8: Morpholino pyrimidine compounds induced apoptosis is associated with ROS production, activation of caspases, chromatin condensation and DNA fragmentation. Intracellular ROS production in HeLa and NCI-H460 cells after treatment with 4c and 5h compounds respectively was determined by fluorescence microscopy using ROS specific fluorescent probe (DCFDA-H2) (A). Activation of executioner caspases (caspase3/7) in HeLa and NCI-H460 cells after treatment with 4c and 5h compounds respectively was determined by measuring caspase 3/7 activity using caspase 3/7 Glo assay and represented as fold increase in activity ***P>0.001 (B). Agarose gel profiles showing DNA fragmentation in HeLa and NCI-H460 cells after treatment with 4c and 5h compounds respectively at different concentrations (0-20μM) (C). DAPI-staining showing the chromatin-condensed nuclei in apoptotic cells following treatment with 4c and 5h compounds. (D). "M" is marker

34x43mm (300 x 300 DPI)

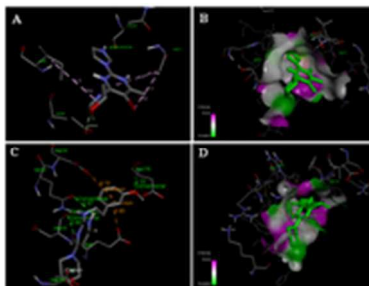
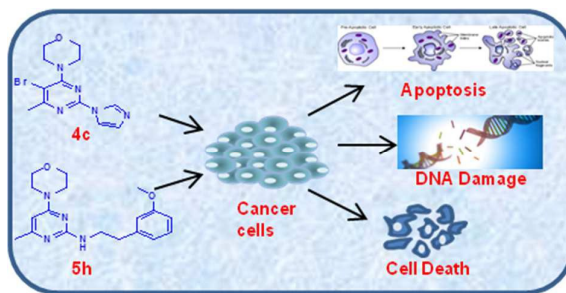


Figure 9: Docking analysis of 4c and 5h shows the binding of these molecules at the binding domain of the mTOR molecule. 4C at the binding domain of the mTOR shows interactions with the neighbouring amino acids (A). Surface around the 4c molecule interacting with the mTOR molecule (B). 5h at the binding domain of the mTOR showing interactions with the neighbouring amino acids (C). Surface around the 5h molecule interacting with the mTOR molecule (D).

15x12mm (300 x 300 DPI)



A series of 4-Methyl-6-morpholinopyrimidine derivatives were synthesised and found to prevent cancer cell proliferation by inducing apoptosis